

Accounting for the species-dependence of the 3500 cm⁻¹ H₂O_t infrared molar absorptivity coefficient: Implications for hydrated volcanic glasses [‡]

IONA M. MCINTOSH^{1,*}, ALEXANDER R.L. NICHOLS^{1,†}, KENICHIRO TANI², AND EDWARD W. LLEWELLIN³

¹Japan Agency for Marine-Earth Science and Technology (JAMSTEC), 2-15 Natsushima-cho, Yokosuka, Kanagawa 237-0061, Japan

²Department of Geology and Paleontology, National Museum of Nature and Science, 4-1-1 Amakubo, Tsukuba, Ibaraki 305-0005, Japan

³Department of Earth Sciences, Durham University, Durham DH1 3LE, U.K.

ABSTRACT

Fourier transform infrared (FTIR) spectroscopy can be used to determine the concentration and speciation of dissolved water in silicate glasses if the molar absorptivity coefficients (ϵ) are known. Samples that are thin and/or water-poor typically require the use of the mid-IR 3500 cm⁻¹ total water (H₂O_t) and 1630 cm⁻¹ molecular water (H₂O_m) absorbance bands, from which hydroxyl water (OH) must be determined by difference; however, accurate determination of H₂O_t and OH is complicated because ϵ_{3500} varies with water speciation, which is not usually known a priori. We derive an equation that uses end-member ϵ_{3500} values to find accurate H₂O_t and OH concentrations from the 3500 cm⁻¹ absorbance for samples where only the H₂O_m concentration need be known (e.g., from the 1630 cm⁻¹ band). We validate this new species-dependent ϵ_{3500} method against published data sets and new analyses of glass standards. We use published data to calculate new end-member ϵ_{3500} values of $\epsilon_{3500_{OH}} = 79 \pm 11$ and $\epsilon_{3500_{H_2O_m}} = 49 \pm 6$ L/mol-cm for Fe-bearing andesite and $\epsilon_{3500_{OH}} = 76 \pm 12$ and $\epsilon_{3500_{H_2O_m}} = 62 \pm 7$ L/mol-cm for Fe-free andesite. These supplement existing end-member values for rhyolite and albite compositions. We demonstrate that accounting for the species-dependence of ϵ_{3500} is especially important for hydrated samples, which contain excess H₂O_m, and that accurate measurement of OH concentration, in conjunction with published speciation models, enables reconstruction of original pre-hydration water contents. Although previous studies of hydrous silicate glasses have suggested that values of ϵ decrease with decreasing tetrahedral cation fraction of the glass, this trend is not seen in the four sets of end-member ϵ_{3500} values presented here. We expect that future FTIR studies that derive end-member ϵ_{3500} values for additional compositions will therefore not only enable the species-dependent ϵ_{3500} method to be applied more widely, but will also offer additional insights into the relationship between values of ϵ and glass composition.

Keywords: FTIR, water, H₂O speciation, volcanic glass, rhyolite, andesite, hydration, obsidian

INTRODUCTION

The dissolved water content of a silicate melt affects a range of magmatic processes, since it exerts a strong influence on melt viscosity (e.g., Hess and Dingwell 1996; Giordano et al. 2008), volatile diffusivities (e.g., Baker et al. 2005; Baker and Alletti 2012), and crystallization (e.g., Hammer 2004; Gualda et al. 2012). Accurate measurement of the water content of silicate glasses is therefore crucial to a wide range of volcanological and petrological studies. Additionally, measuring water speciation, i.e., the amount of water present as molecular water (H₂O_m) vs. hydroxyl groups (OH), can provide information about the cooling rate and glass transition temperature (T_g) of a sample (e.g., Stolper 1989; Dingwell and Webb 1990; Xu and Zhang 2002), and whether a sample has been affected by hydration during bubble resorption, or crystallization during cooling (e.g., McIntosh et al. 2014; Nichols et al. 2014), or by secondary hydration at low temperature in the time following deposition (e.g., Dixon et al. 1995; Anovitz et

al. 2008; Denton et al. 2009; Tuffen et al. 2010). Whereas most commonly used techniques [e.g., hydrogen manometry, thermogravimetric analysis (TGA), secondary ion mass spectrometry (SIMS)] can measure only total water (H₂O_t) contents, Fourier transform infrared spectroscopy (FTIR) is capable of measuring both total water and water species concentrations.

FTIR ANALYSIS OF HYDROUS GLASSES

During transmission FTIR analysis, some infrared light passing through the sample is absorbed by molecules within the sample, with different species absorbing light at different, characteristic frequencies. The resulting FTIR spectrum thus exhibits absorbance bands at wavelengths (or wavenumbers, cm⁻¹) corresponding to these different absorbing species. There are four main absorbance bands associated with water dissolved in silicate glasses that can be seen in the near- and mid-IR range (Fig. 1), and their assignments are given in Table 1. The H₂O_m and OH bands at 5200 and 4500 cm⁻¹ have low absorption intensities and are often not detected in glasses that have low water contents or that require thin samples for analysis (e.g., to avoid bubbles or crystals in the beampath). Additionally, these bands can be difficult to measure accurately in intermediate glass compositions where absorptions

* E-mail: i.m.mcintosh@jamstec.go.jp

† Present address: Department of Geological Sciences, University of Canterbury, Private Bag 4800, Christchurch 8140, New Zealand.

‡ Open access: Article available to all readers online.

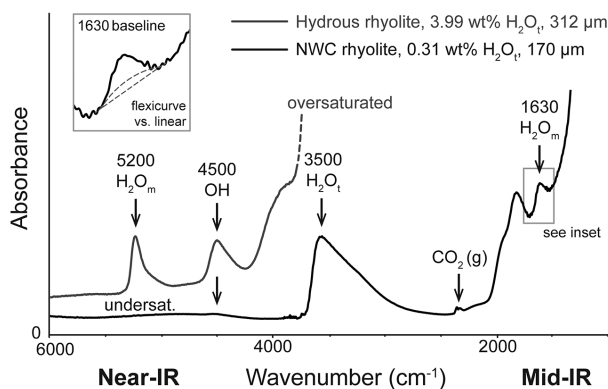


FIGURE 1. H_2O absorbance bands in FTIR spectra of hydrous rhyolite glasses. The 5200 and 4500 cm^{-1} bands can be seen in the thick, water-rich glass (gray spectrum), but the mid-IR bands are oversaturated. In the thinner, water-poor NWC glass (black spectrum, this study), the 5200 cm^{-1} band is undersaturated and the 4500 cm^{-1} band is only weakly seen, but the 3500 and 1630 cm^{-1} bands can be seen. A small doublet can be seen at ~ 2350 cm^{-1} due to molecular CO_2 in the atmosphere. Inset compares choice of linear and flexicurve baselines for 1630 cm^{-1} band.

TABLE 1. Assignments of the major H_2O IR absorbance bands in silicate glasses

Band	Assignment
5200 cm^{-1}	Combination stretching and bending modes of water molecules
4500 cm^{-1}	Combination stretching and bending modes of structural SiOH and AlOH groups
3500 cm^{-1}	Fundamental OH stretching vibration of both water molecules and structural SiOH and AlOH groups, with the distribution of H-bond strengths between the different species causing the band's breadth and asymmetry
1630 cm^{-1}	Fundamental bending mode of water molecules

by Fe cause curvature of the baseline at high wavenumbers (e.g., Stolper 1982b; Ohlhorst et al. 2001; Mandeville et al. 2002), or for samples where the absorptions creating the 4500 cm^{-1} band may be complex (Malfait 2009; Le Losq et al. 2015). In many situations therefore the 3500 cm^{-1} band is used to measure the total water (H_2O_i) concentration, and water speciation is obtained by measuring the 1630 cm^{-1} H_2O_m band and then finding OH indirectly by difference (e.g., Wysoczanski and Tani 2006; Yokoyama et al. 2008; Nichols et al. 2009; McIntosh et al. 2014; Giachetti et al. 2015).

The intensity of the absorbance bands is typically measured as the height of the absorbance peak above the baseline and is termed the absorbance. These absorbance values are then converted into concentrations via the Beer-Lambert law, which relates the attenuation (absorbance) of light passing through a material to the thickness of the material and the concentration of the absorbing species within it, according to:

$$C = \frac{100MA}{\rho l \epsilon} \quad (1)$$

where C is the concentration of the species of interest ($C_{\text{H}_2\text{O}_i}$, $C_{\text{H}_2\text{O}_m}$, or C_{OH} in wt%), M is the molecular weight (in g/mol; 18.02 for water), A is the absorbance (no units), ρ is the density (in g/L), l is the thickness of the analyzed area (in cm), and ϵ is the molar absorptivity coefficient for the absorbance band of interest (in L/mol-cm). If the intensity of the absorbance band is measured

using the area enclosed by the peak and the baseline rather than the peak height, then this is termed the integrated absorbance (in cm^{-1}) and ϵ in Equation 1 is replaced with ϵ^* , the integrated molar absorptivity (in L/mol-cm²). Since the value of the peak area is more sensitive to errors in fitting the baseline than the peak height, it is more common to use the absorbance rather than the integrated absorbance. Values of ϵ (and ϵ^*) are experimentally determined, and, for a given water absorbance band will vary with the anhydrous glass composition, such as from basalt to rhyolite (Silver et al. 1990; Dixon et al. 1995; Ohlhorst et al. 2001; Mandeville et al. 2002; Seaman et al. 2009; Mercier et al. 2010). Establishing the correct value of ϵ to use for a given species in glass of a given composition is therefore fundamental to the quantitative use of FTIR spectroscopy.

It has been previously noted that, because the 3500 cm^{-1} absorbance band is the net result of absorptions by both H_2O_m and OH species (Table 1), the correct molar absorptivity coefficient for that band—termed ϵ_{3500} —will vary with the ratio of the two species (Newman et al. 1986; Okumura et al. 2003). Since the equilibrium proportions of water species vary with temperature and total water concentration (e.g., Stolper 1982a, 1989), and can be altered by disequilibrium processes such as quench resorption (McIntosh et al. 2014), crystallization (e.g., Nichols et al. 2014), and secondary hydration (e.g., Dixon et al. 1995; Anovitz et al. 2008; Tuffen et al. 2010), the “true” ϵ_{3500} value will also vary accordingly, potentially even across the same sample. This accounts for the wide range in ϵ_{3500} values reported in the literature, even among glasses of the same composition. For example, rhyolites, which are the most studied composition to date, have reported ϵ_{3500} values ranging from 75 to 95 L/mol-cm (Table 2).

Newman et al. (1986) show that end-member molar absorptivity coefficients can be calculated for the 3500 cm^{-1} band; these give the theoretical ϵ_{3500} value if all water within the glass were present exclusively as H_2O_m ($\epsilon_{3500, \text{H}_2\text{O}_m}$), or exclusively as OH ($\epsilon_{3500, \text{OH}}$). They demonstrate that these coefficients can be used to determine an accurate species-dependent ϵ_{3500} value, according to:

$$\epsilon_{3500} = X_{\text{OH}} \epsilon_{3500, \text{OH}} + X_{\text{H}_2\text{O}_m} \epsilon_{3500, \text{H}_2\text{O}_m} \quad (2)$$

where X_{OH} and $X_{\text{H}_2\text{O}_m}$ are the simple mass fractions of water dissolved as OH or H_2O_m , respectively. For their data set of hydrous rhyolite compositions, Newman et al. (1986) calculate that $\epsilon_{3500, \text{OH}} = 100 \pm 2$ and $\epsilon_{3500, \text{H}_2\text{O}_m} = 56 \pm 4$ L/mol-cm. However, as the authors point out, this simple relationship for calculating a species-dependent ϵ_{3500} value is of limited analytical use since it requires that the speciation of the sample is already known. This requirement has to date limited the practical use of a species-dependent ϵ_{3500} value and many researchers have instead necessarily, albeit somewhat arbitrarily, selected a constant value from the literature. Here we build on the work of Newman et al. (1986) and present a new methodology for accounting for the species-dependence of ϵ_{3500} , without requiring a priori knowledge of the species proportions. This method enables accurate water species concentrations to be determined from the 3500 and 1630 cm^{-1} absorbance bands. We demonstrate the effectiveness of this technique by applying it to published data sets and to the analyses of glass standards with known water contents, and then discuss its implications for the analysis of hydrated glasses.

TABLE 2. H₂O molar absorptivity coefficients for rhyolite, Fe-bearing and Fe-free andesite, and albite compositions

Composition	τ	NBO/T	ϵ_{5200}	ϵ_{4500}	Fixed ϵ_{3500}	End-member ϵ_{3500}		ϵ_{1630}	Reference	
						$\epsilon_{3500_{OH}}$	$\epsilon_{3500_{H_2O_m}}$			
Rhyolite	0.859	0.02	1.61 ± 0.05	1.73 ± 0.02		100 ± 2	56 ± 4	55 ± 2	N: (1) O: (2) I: (3) L: (4) D: (5) H: (6) A: (7) ON: (8)	
			1.86 ± 0.05	1.50 ± 0.10	75 ± 4					
					80 ± 4					
					80 ± 4.9 ^b					
					88 ± 2					
Fe-bearing andesite	0.746	0.32	1.75 ± 0.08	1.42 ± 0.12		79 ± 11	49 ± 6		This study ^a M: (9) K: (10)	
			1.07 ± 0.07	0.79 ± 0.07	62.32 ± 0.42			42.34 ± 2.77		
			1.08 ± 0.11	1.15 ± 0.17	70.32 ± 6.86			40.83 ± 4.12		
Fe-free andesite	0.795	0.18	1.46 ± 0.07	0.89 ± 0.07	69.21 ± 0.52	76 ± 12	62 ± 7	52.05 ± 2.85	This study ^a (9) (11)	
			1.04 ± 0.04	0.92 ± 0.03						
Albite	0.800	0.00	1.67 ± 0.06	1.13 ± 0.04	70 ± 2	69 ± 17	71 ± 17	49 ± 2	This study ^a (12)	

Notes: Published coefficients are from (1) Newman et al. (1986), (2) Okumura et al. (2003), (3) Ihinger et al. (1994), (4) Leschik et al. (2004), (5) Dobson et al. (1989), (6) Hauri et al. (2002), (7) Aubaud et al. (2009), (8) Okumura and Nakashima (2005), (9) Mandeville et al. (2002), (10) King et al. (2002), (11) Vetere et al. (2006), and (12) Silver and Stolper (1989). $\tau = (Si^{4+} + Al^{3+}) / \text{total cations}$, as calculated by Mandeville et al. (2002). NBO/T is the ratio of non-bridging O atoms over tetrahedrally coordinated cations.

^a End-member ϵ_{3500} values derived during this study are based on the data sets of (9) Mandeville et al. (2002) (Fe-bearing and Fe-free andesite compositions) and (12) Silver and Stolper (1989) (albite composition).

^b For H₂O_T < 2 wt%; for H₂O_T > 2 wt% $\epsilon_{3500} = 80 (\pm 1) - 1.36 (\pm 0.23) C_{H_2O_t}$, where $C_{H_2O_t}$ is H₂O_T concentration in wt% (Leschik et al. 2004).

ACCOUNTING FOR SPECIES-DEPENDENCE OF ϵ_{3500}

Calculation of OH concentration using end-member ϵ_{3500} values

Equation 2 can be rewritten in terms of species concentrations, using the definitions $X_{OH} = C_{OH}/C_{H_2O_t}$ and $X_{H_2O_m} = C_{H_2O_m}/C_{H_2O_t}$, giving

$$\epsilon_{3500} = \frac{C_{OH}\epsilon_{3500_{OH}} + C_{H_2O_m}\epsilon_{3500_{H_2O_m}}}{C_{H_2O_t}} \quad (3)$$

Rearranging for $C_{H_2O_t}$ and substituting into the Beer-Lambert law (Eq. 1), we obtain an expression for the concentration of OH

$$C_{OH} = \frac{1}{\epsilon_{3500_{OH}}} \left(\frac{100 M \bar{A}_{3500}}{\rho} - \epsilon_{3500_{H_2O_m}} C_{H_2O_m} \right) \quad (4)$$

where \bar{A}_{3500} is the measured 3500 cm⁻¹ absorbance normalized for sample thickness (i.e., $\bar{A} = A/l$) in units of 1/cm. With this equation it is now possible to calculate directly the OH concentration of a sample if the glass thickness, 3500 cm⁻¹ absorbance, H₂O_m concentration (which can be found from either the 5200 or 1630 cm⁻¹ absorbance band in the conventional way via Eq. 1), and the end-member ϵ_{3500} values for the glass composition of interest are known. H₂O_T concentration is then simply $C_{H_2O_t} = C_{OH} + C_{H_2O_m}$.

To test the accuracy of this new species-dependent ϵ_{3500} method we apply it to the published data set of Newman et al. (1986) from which they calculated their end-member ϵ_{3500} values for rhyolite. Their data set consists of samples of natural rhyolitic obsidian from tephra deposits, domes, and flows taken from a range of locations in the U.S.A. Thickness data and 5200, 4500, and 3500 cm⁻¹ absorbances are reported for 28 analyses of 24 different samples, containing 0.27–2.64 wt% H₂O_T as measured by manometry. For these samples, we calculate their H₂O_T and OH concentrations in the conventional way (Eq. 1) using the published

5200 cm⁻¹ (H₂O_m) and 4500 cm⁻¹ (OH) absorbance data together with the ϵ_{5200} and ϵ_{4500} values for rhyolite derived by Newman et al. in the same study (Table 2). These are then plotted against the H₂O_T and OH concentrations of the same samples calculated from the published 3500 cm⁻¹ (H₂O_T) and 1630 cm⁻¹ (H₂O_m) absorbances using our new species-dependent method with the values of $\epsilon_{3500_{OH}}$ and $\epsilon_{3500_{H_2O_m}}$ for rhyolite derived by Newman et al. (Fig. 2). We find that there is excellent agreement between H₂O_T and OH concentrations calculated by the two methods, as demonstrated by the excellent fit to the 1:1 line ($R^2 = 0.993$ for H₂O_T, and $R^2 = 0.971$ for OH). The “true” (species-dependent) ϵ_{3500} values for individual samples then calculated via Equation 2 range from 73.6 to 97.2 L/mol·cm, compared to the end-member values of $\epsilon_{3500_{OH}} = 100 \pm 2$ and $\epsilon_{3500_{H_2O_m}} = 56 \pm 4$ L/mol·cm.

Calculating end-member ϵ_{3500} values for different compositions

New end-member ϵ_{3500} values can be calculated for different glass compositions following the procedure of Newman et al. (1986), who showed that the absorbances of the 5200, 4500, and 3500 cm⁻¹ bands and their molar absorptivity coefficients can be related as:

$$\bar{A}_{3500} = \frac{\epsilon_{3500_{H_2O_m}}}{\epsilon_{5200}} \bar{A}_{5200} + \frac{\epsilon_{3500_{OH}}}{\epsilon_{4500}} \bar{A}_{4500} \quad (5)$$

This has the form $y = m_1x_1 + m_2x_2$, thereby enabling the use of multiple linear regression (e.g., using the Linest function in Microsoft Excel) to find the values of $\epsilon_{3500_{H_2O_m}}/\epsilon_{5200}$ and $\epsilon_{3500_{OH}}/\epsilon_{4500}$ from the measured 5200 and 4500 cm⁻¹ absorbances. Values of ϵ_{5200} and ϵ_{4500} reported in the literature can then be used to find the two unknowns, i.e., the end-member coefficients $\epsilon_{3500_{H_2O_m}}$ and $\epsilon_{3500_{OH}}$.

Thus to calculate end-member ϵ_{3500} values for a given glass composition, it is necessary to have a data set containing 5200, 4500, and 3500 cm⁻¹ absorbance and thickness data for the same piece(s) of glass, for which the ϵ_{5200} and ϵ_{4500} values are also known. Since the absorbances are normalized to thickness it is

possible to measure the weaker 5200 and 4500 cm^{-1} absorbances on a thicker piece of glass and then subsequently thin it to measure the 3500 cm^{-1} absorbance. Additionally, it would also be possible to use the 1630 cm^{-1} $\text{H}_2\text{O}_\text{m}$ absorbance and ϵ_{1630} value in place of the 5200 cm^{-1} $\text{H}_2\text{O}_\text{m}$ absorbance and ϵ_{5200} value, if necessary.

We demonstrate this procedure by using the published data set of Mandeville et al. (2002)

to calculate new end-member ϵ_{3500} values for both their Fe-bearing and Fe-free andesite compositions. Their samples are hydrous glasses that were synthesized at high pressure and temperature from either a mixture of natural basaltic andesite and evolved andesite rock powders from Krakatau, or a mixture of pure oxide powders and carbonates; $\text{H}_2\text{O}_\text{t}$ contents were measured by hydrogen manometry (see original study for further details). In their data set, glasses with data for all three bands (5200, 4500, and 3500 cm^{-1}) include two Fe-bearing andesite glasses, Run 9 (1030 $^\circ\text{C}$, 200 MPa, 4.32 wt% $\text{H}_2\text{O}_\text{t}$, 28 analyses) and Run 101 (1100 $^\circ\text{C}$, 50 MPa, 1.67 wt% $\text{H}_2\text{O}_\text{t}$, 13 analyses), and three Fe-free andesite glasses, Run 58 (1100 $^\circ\text{C}$, 200 MPa, 5.68 wt% $\text{H}_2\text{O}_\text{t}$, 56 analyses), Run 68 (1100 $^\circ\text{C}$, 150 MPa, 2.15 wt% $\text{H}_2\text{O}_\text{t}$, 11 analyses), and Run 106 (1050 $^\circ\text{C}$, 65 MPa, 1.31 wt% $\text{H}_2\text{O}_\text{t}$, 9 analyses). From the normalized absorbances of these glasses we used the Linest function in Microsoft Excel to find values of $\epsilon_{3500_{\text{H}_2\text{O}_\text{m}}}/\epsilon_{5200}$ and $\epsilon_{3500_{\text{OH}}}/\epsilon_{4500}$, as per Equation 5, for each composition, from which the end-member $\epsilon_{3500_{\text{OH}}}$ and $\epsilon_{3500_{\text{H}_2\text{O}_\text{m}}}$ coefficients were calculated using the values of ϵ_{5200} and ϵ_{4500} previously derived and published in the original study (Table 2).

For the Fe-bearing andesite glass compositions reported in Mandeville et al. we thus calculate end-member ϵ_{3500} values of $\epsilon_{3500_{\text{OH}}} = 79 \pm 11$ and $\epsilon_{3500_{\text{H}_2\text{O}_\text{m}}} = 49 \pm 6$ L/mol·cm, while for their Fe-free andesite composition we calculate values of $\epsilon_{3500_{\text{OH}}} = 76 \pm 12$ and $\epsilon_{3500_{\text{H}_2\text{O}_\text{m}}} = 62 \pm 7$ L/mol·cm. Errors were calculated by propagating the standard error on the regression coefficients and the reported error on the ϵ_{5200} and ϵ_{4500} values used to derive them via Equation 5. Figure 3 compares the $\text{H}_2\text{O}_\text{t}$ and OH concentrations calculated from the 5200 and 4500 cm^{-1} bands with those calculated from the 3500 and 1630 cm^{-1} bands using both the species-dependent ϵ_{3500} method (Eq. 4) with the new end-member ϵ_{3500} values (filled symbols) and the conventional method (Eq. 1) with the fixed ϵ_{3500} value derived by Mandeville et al. (open symbols). For both compositions, the $\text{H}_2\text{O}_\text{t}$ concentrations calculated using the species-dependent ϵ_{3500} method are in slightly better agreement with the $\text{H}_2\text{O}_\text{t}$ concentrations calculated from the 5200 and 4500 cm^{-1} bands than the data calculated using the fixed ϵ_{3500} value (Figs. 3a and 3c). Meanwhile, the OH concentrations calculated using the species-

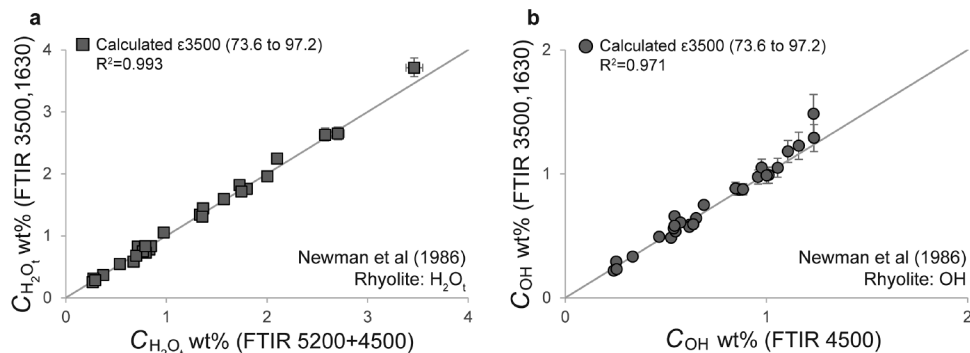


FIGURE 2. Validation of the species-dependent ϵ_{3500} method for rhyolite. $\text{H}_2\text{O}_\text{t}$ (squares) and OH (circles) concentrations calculated from the 3500 and 1630 cm^{-1} bands using the species-dependent ϵ_{3500} method (i.e., with $\text{H}_2\text{O}_\text{m}$ concentration calculated from the 1630 cm^{-1} band via Eq. 1 and used as an input for Eq. 4 to calculate OH concentration, hence $\text{H}_2\text{O}_\text{t}$ concentration) are compared to those derived from the 5200 and 4500 cm^{-1} bands for the published data set of Newman et al. (1986). Solid line indicates the 1:1 line. Error bars calculated by propagating uncertainties on all values of ϵ .

dependent ϵ_{3500} method are in markedly better agreement with the OH concentrations calculated from the 4500 cm^{-1} band than those calculated from the 3500 cm^{-1} band using the conventional OH-by-difference method. For Fe-bearing andesite the OH-by-difference method gives no correlation with OH concentrations derived directly from the 4500 cm^{-1} band ($R^2 = 0.10$), whereas the new method gives a much better fit ($R^2 = 0.80$; Fig. 3b). The OH data for Fe-free andesite are somewhat more scattered with regards to the 1:1 line, with most of the scatter corresponding to one glass (Run 58a), but the new method again is closer to the gradient of the 1:1 line and provides a better correlation than the OH-by-difference method, with R^2 values of 0.66 and 0.55, respectively (Fig. 3d).

A previous study by Silver and Stolper (1989) of H_2O in albitic glasses also followed the method of Newman et al. (1986) in determining end-member ϵ_{3500} values for the 3500 cm^{-1} band, but since they were similar they elected to publish a single fixed ϵ_{3500} value instead. For completeness, we use the published Silver and Stolper data set (absorbance data for 5 glasses, synthesized at 1500–2000 MPa and 1400–1600 $^\circ\text{C}$ with 1.02–5.12 wt% $\text{H}_2\text{O}_\text{t}$) to calculate that the end-member ϵ_{3500} values would be $\epsilon_{3500_{\text{OH}}} = 69 \pm 17$ and $\epsilon_{3500_{\text{H}_2\text{O}_\text{m}}} = 71 \pm 17$ L/mol·cm, compared to the published fixed ϵ_{3500} value of 70 ± 2 L/mol·cm (Table 2).

Application to hydrous glass standards

To further test the accuracy of Equation 4 we performed transmission FTIR analyses of three glass standards with independently constrained water contents (NWC, KRA-045-2, Run 10). Chemical compositions and densities of these glasses are reported in Table 3. NWC is a rhyolitic obsidian from the Upper Dome of NW Coulee at Mono Craters, California. A piece of this glass was included in the data set of Hauri et al. (2002) (“NW Coulee”), whose manometry analysis found it to contain 0.297 wt% $\text{H}_2\text{O}_\text{t}$. KRA-045-2 is a rhyodacitic obsidian matrix glass from the pyroclastic flow deposit of the 1883 Krakatau eruption (Mandeville et al. 1998), which was analyzed by manometry and found to contain 0.48 wt% $\text{H}_2\text{O}_\text{t}$ [C. Mandeville, published in Maria and Luhr (2008)]. Finally, Run 10 is an experimentally synthesized Fe-bearing andesite glass that was part of the data set of Mandev-

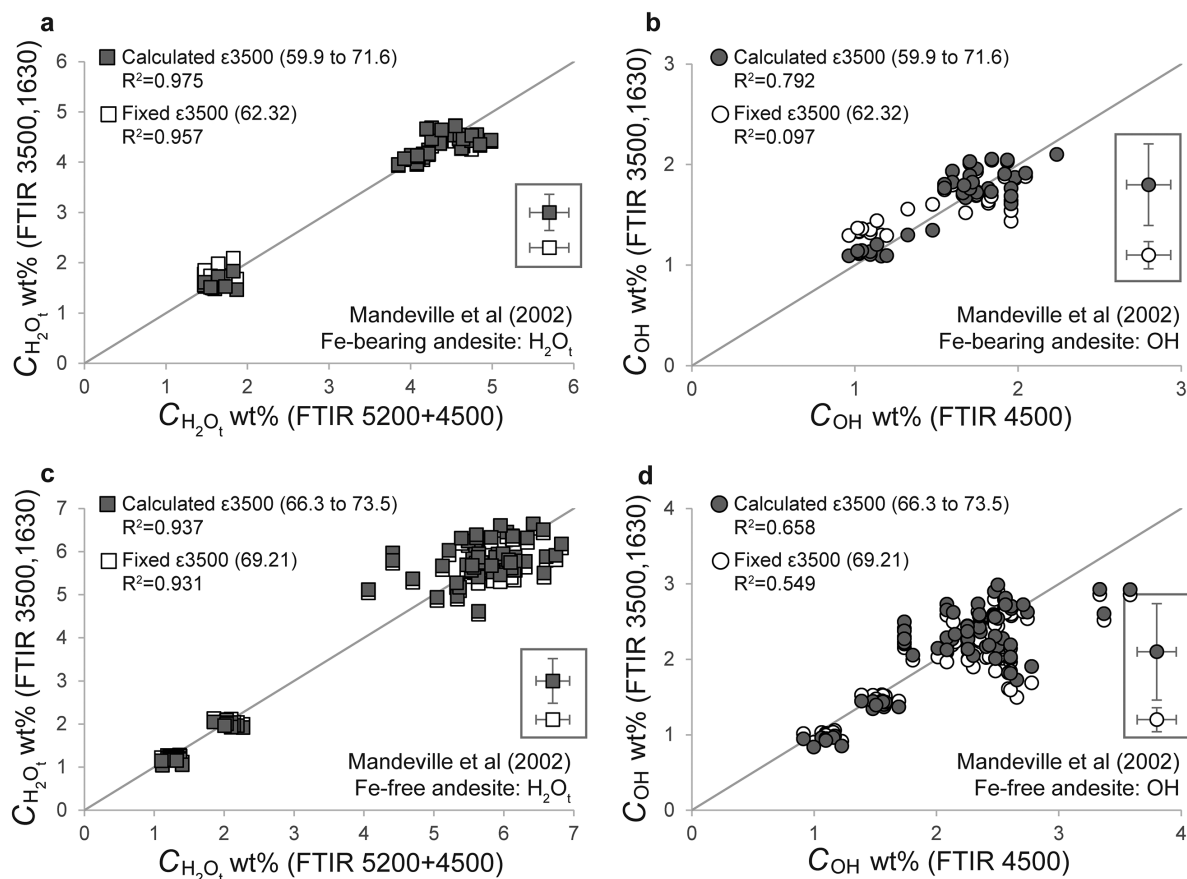


FIGURE 3. Validation of the species-dependent ϵ_{3500} method for andesite. H₂O_t (squares) and OH (circles) concentrations calculated from the 3500 and 1630 cm⁻¹ bands using the species-dependent ϵ_{3500} method (filled symbols) are compared to those derived from the 5200 and 4500 cm⁻¹ bands for the published data set of Mandeville et al. (2002) for (a and b) Fe-bearing andesite and (c and d) Fe-free andesite. H₂O_t and OH-by-difference concentrations calculated using the fixed ϵ_{3500} values of the Mandeville et al. study are shown for comparison (open symbols). Solid line indicates the 1:1 line. For clarity, errors calculated from uncertainties on all values of ϵ used by each method are shown as symbols with representative error bars on the right-hand margin of each figure tile.

ille et al. (2002), whose manometry analysis gives its total water content as 5.78 wt% H₂O_t.

METHODS

All three glasses were prepared for transmission FTIR analysis as double-polished free-standing wafers. The glass thicknesses of the rhyolite standards (NWC and KRA-045-2) were measured using a digital micrometer with a precision of $\pm 1 \mu\text{m}$, with measurements taken at the location of each analysis. Run 10 was too thin, hence fragile, to measure with the micrometer and so thickness was instead calculated from fringes in reflectance spectra following the method of Wysoczanski and Tani (2006) and utilizing a refractive index of 1.55 for andesite (Wohletz and Heiken 1992), with an estimated accuracy of $\pm 3 \mu\text{m}$. FTIR spot analyses were performed at the Japan Agency for Marine-Earth Science and Technology, using a Varian FTS 7000 spectrometer and an attached UMA600 microscope. Mid-IR (6000–700 cm⁻¹) transmittance spectra were collected over 512 scans at a resolution of 8 cm⁻¹ using a heated ceramic IR source, a KBr beamsplitter and a liquid nitrogen-cooled HgCdTe₂ (MCT) detector. Apertures were used to reduce the beam spot size to 20 × 20 μm . Both the spectrometer bench and microscope were continuously purged with N₂ gas to minimize any interference from atmospheric H₂O. Obtained spectra were then processed using Win-IR Pro software. Band absorbances were determined by measuring the height of the peak above the baseline. For the 3500 cm⁻¹ band a linear baseline was used, while for the 4500 and 1630 cm⁻¹ bands baselines were drawn by hand using a flexicurve. H₂O_m concentration was calculated from the 1630 cm⁻¹

TABLE 3. Rhyolite and Fe-bearing andesite hydrous glass standards

Oxide wt%	NWC	KRA-045-2	Run 10
SiO ₂	76.45	72.17(22)	57.18(66)
TiO ₂	0.06	0.53(02)	1.08(04)
Al ₂ O ₃	12.32	14.07(08)	16.24(34)
FeO ^a	1.02	2.62(07)	4.75(33)
MnO	0.06	0.13(05)	0.00(-)
MgO	0.01	0.57(03)	3.28(07)
CaO	0.52	1.79(06)	7.39(13)
Na ₂ O	3.80	5.27(28)	3.01(09)
K ₂ O	4.75	2.46(13)	1.27(05)
P ₂ O ₅	0.00	0.00(-)	0.00(-)
H ₂ O _t (manometry)	0.297	0.48	5.78
Total	99.29	100.09	99.98
Density (g/L)	2340	2395	2510
Wafer thickness (μm)	150–170	151	21

Notes: NWC composition from M. Humphreys (pers. comm.), manometry from Hauri et al. (2002), density from Newman et al. (1986); KRA-045-2 composition from M. Humphreys (personal communication), manometry and density from Maria and Luhr (2008); Run 10 composition, manometry, and density from Mandeville et al. (2002). Wafer thickness measured at each FTIR analysis location by micrometer for NWC and KRA-045-2, and by interference fringes in reflectance FTIR spectra for Run 10. Standard deviations where known are given in parentheses in terms of least units reported, e.g., 72.17(22) indicates a standard deviation of 0.22 wt%.

^a Total Fe as FeO.

absorbance via the Beer-Lambert law (Eq. 1) using ϵ 1630 values of 55 ± 2 L/mol·cm for rhyolite (Newman et al. 1986) and 42.34 ± 2.77 L/mol·cm for Fe-bearing andesite (Mandeville et al. 2002). OH concentration was then calculated according to Equation 4, utilizing the end-member ϵ 3500 values of Newman et al. (1986) for rhyolite and the newly derived end-member ϵ 3500 values for Fe-bearing andesite. $\text{H}_2\text{O}_\text{t}$ was then calculated as $C_{\text{H}_2\text{O}_\text{t}} = C_{\text{OH}} + C_{\text{H}_2\text{O}_\text{m}}$. For comparison, $C_{\text{H}_2\text{O}_\text{t}}$ and C_{OH} (using OH-by-difference) were also calculated from the 3500 cm^{-1} band via Equation 1 using the range of published fixed ϵ 3500 values (Table 2). For NWC and KRA-045-2 OH concentration was also calculated via Equation 1 from the 4500 cm^{-1} band using appropriate values of ϵ 4500 (Table 2).

RESULTS

Table 4 and Figures 4 and 5 show the results of the FTIR spot analyses of the two rhyolite standards, NWC and KRA-045-2, and the Fe-bearing andesite Run 10. Reported values for each sample are the mean value of 12 measurements made on the same wafer. Errors for the rhyolite standards are given as one standard deviation and for the Fe-bearing andesite are derived from the ± 3 μm error on the thickness measurement, which becomes the dominant source of error for thin samples. For each glass, the $\text{H}_2\text{O}_\text{t}$ concentration measured by FTIR using both the species-dependent ϵ 3500 method and the conventional fixed ϵ 3500 method is plotted against their known $\text{H}_2\text{O}_\text{t}$ content previously measured by manometry (Figs. 4a and 5a). For all compositions, the species-dependent ϵ 3500 method (filled squares) gives $\text{H}_2\text{O}_\text{t}$ concentrations that are within 5% of the known value, whereas those calculated using fixed ϵ 3500 values from the literature (open squares) span a wide range and differ from the known $\text{H}_2\text{O}_\text{t}$ concentration by as much as 33%.

OH concentrations calculated using the species-dependent ϵ 3500 method and the conventional OH-by-difference method are compared to the OH concentration obtained from the 4500 cm^{-1} band (Figs. 4b and 5b). For each glass, $\text{H}_2\text{O}_\text{t}$ concentrations determined by summing the 4500 cm^{-1} OH and 1630 cm^{-1} $\text{H}_2\text{O}_\text{m}$ concentrations were compared to their manometry $\text{H}_2\text{O}_\text{t}$ concentration (Fig. 4c), with the fit to the 1:1 line used to select the most appropriate ϵ 4500 value from the literature (Table 2). Since the weak 4500 cm^{-1} band could not be measured in our thin Run 10 standard we use instead the 4500 cm^{-1} absorbance data reported by Mandeville et al. (2002) for the same glass, and the ϵ 4500 value derived in the same study (Table 2). For the rhyolite standards (Fig. 4b) the OH concentrations calculated by the species-dependent ϵ 3500 method (filled circles) are within 12% of the 4500 cm^{-1} OH concentration for NWC and within 2% for KRA-045-2, whereas the OH-by-difference concentrations using fixed ϵ 3500 values (open circles) differ by up to 45% and 27%, respectively. For the Fe-bearing andesite Run 10 (Fig. 5b), the species-dependent ϵ 3500 method gives an OH concentration within 9% of that reported by Mandeville et al. (2002). Finding OH-by-difference using the fixed ϵ 3500 value derived by Mandeville et al. (2002) (for the data set that contained Run 10) matches

the 4500 cm^{-1} value exactly, whereas the OH-by-difference derived using the King et al. (2002) fixed ϵ 3500 coefficient is 39% lower than the 4500 cm^{-1} value.

DISCUSSION

Accuracy of $\text{H}_2\text{O}_\text{t}$ and OH concentrations from species-dependent ϵ 3500 method

The new species-dependent ϵ 3500 method is able to reproduce accurately the $\text{H}_2\text{O}_\text{t}$ and OH concentrations of both the published rhyolite and andesite data sets (Figs. 2 and 3) and the hydrous glass standards (Figs. 4 and 5; Table 4). For the data sets, the $\text{H}_2\text{O}_\text{t}$ and OH concentrations derived from the 5200 cm^{-1} $\text{H}_2\text{O}_\text{m}$ and 4500 cm^{-1} OH absorbance bands are not strictly independent measurements since they need ϵ 5200 and ϵ 4500 values to find concentration via the Beer-Lambert law. However, by using the ϵ 5200 and ϵ 4500 values derived from these same data sets in the original studies of Newman et al. (1986) and Mandeville et al. (2002) the resulting concentrations are particularly reliable. The $\text{H}_2\text{O}_\text{t}$ and OH concentrations from the new species-dependent ϵ 3500 method have an excellent correlation with the values derived from the 5200 and 4500 cm^{-1} bands, demonstrating the accuracy of this technique (Figs. 2 and 3). For the andesite data sets, the species-dependent ϵ 3500 method gives a better fit than the conventional method using fixed ϵ 3500 values. Although the improvement for $\text{H}_2\text{O}_\text{t}$ is only slight, it is particularly marked for OH, where the species-dependent ϵ 3500 method gives much better agreement with the 4500 cm^{-1} OH concentrations than the conventional OH-by-difference method. In particular, the OH-by-difference values for Fe-bearing andesite (Fig. 3b) give no meaningful correlation to the 4500 cm^{-1} OH concentrations ($R^2 = 0.10$) while the species-dependent method gives a much stronger correlation ($R^2 = 0.79$). We therefore strongly recommend the use of the species-dependent ϵ 3500 method for finding the OH concentration when it is necessary to use the 3500 absorbance band to do so.

Similarly, FTIR analysis of the three glass standards using the species-dependent ϵ 3500 method produces $\text{H}_2\text{O}_\text{t}$ and OH concentrations that are within 11% of their independently determined concentrations. The absolute difference is greatest for the Fe-bearing andesite Run 10, where the species-dependent ϵ 3500 method overestimates $\text{H}_2\text{O}_\text{t}$ by 0.11 wt% (Fig. 5a). This discrepancy is most likely due to the need to analyze a thin glass wafer (to avoid saturation of the 3500 cm^{-1} band in this water-rich sample), which increases the relative error owing to the thickness measurement and also creates interference fringes, which introduce uncertainty when picking the baseline. Since Run 10 is water-rich however, this error is <2% of the total $\text{H}_2\text{O}_\text{t}$ concentration measured by manometry.

TABLE 4. H_2O absorbance and concentration data from analyses of hydrous glass standards

Sample	n	Normalized absorbance (1/cm)			From 1630 $\text{H}_2\text{O}_\text{m}$ (wt%)	Using species-dependent ϵ 3500 method		From 4500 OH (wt%)	Manometry $\text{H}_2\text{O}_\text{t}$ (wt%)	
		4500 cm^{-1} OH	3500 cm^{-1} $\text{H}_2\text{O}_\text{t}$	1630 cm^{-1} $\text{H}_2\text{O}_\text{m}$		OH (wt%)	$\text{H}_2\text{O}_\text{t}$ (wt%)			ϵ 3500 value
NWC	12	0.552(110)	38.338(2.219)	2.674(443)	0.04(01)	0.27(02)	0.31(02)	94.7(9)	0.25(05)	0.297
KRA-045-2	12	0.790(073)	57.395(1.331)	5.326(898)	0.07(01)	0.39(01)	0.46(01)	93.1(1.1)	0.40(04)	0.48
Run 10	12	–	495.040(3.606)	216.270(5.116)	3.67(09)	2.23(03)	5.89(06)	60.3(3)	2.04(19)	5.78

Notes: Table shows the average normalized absorbance measured by FTIR in this study for each standard glass (n = number of analyses). $\text{H}_2\text{O}_\text{m}$ concentration from the 1630 cm^{-1} band and OH concentration from the 4500 cm^{-1} band are calculated in the conventional manner via the Beer-Lambert law (Eq. 1, see Methods section for details). $\text{H}_2\text{O}_\text{m}$ concentration from the 1630 cm^{-1} band is used in the species-dependent ϵ 3500 method (Eq. 4) to calculate the OH and $\text{H}_2\text{O}_\text{t}$ concentrations and “true” ϵ 3500 value of each glass. $\text{H}_2\text{O}_\text{t}$ concentrations determined for each glass by manometry are shown for comparison (see Table 3 for details). Standard deviations are given in parentheses in terms of least units reported.

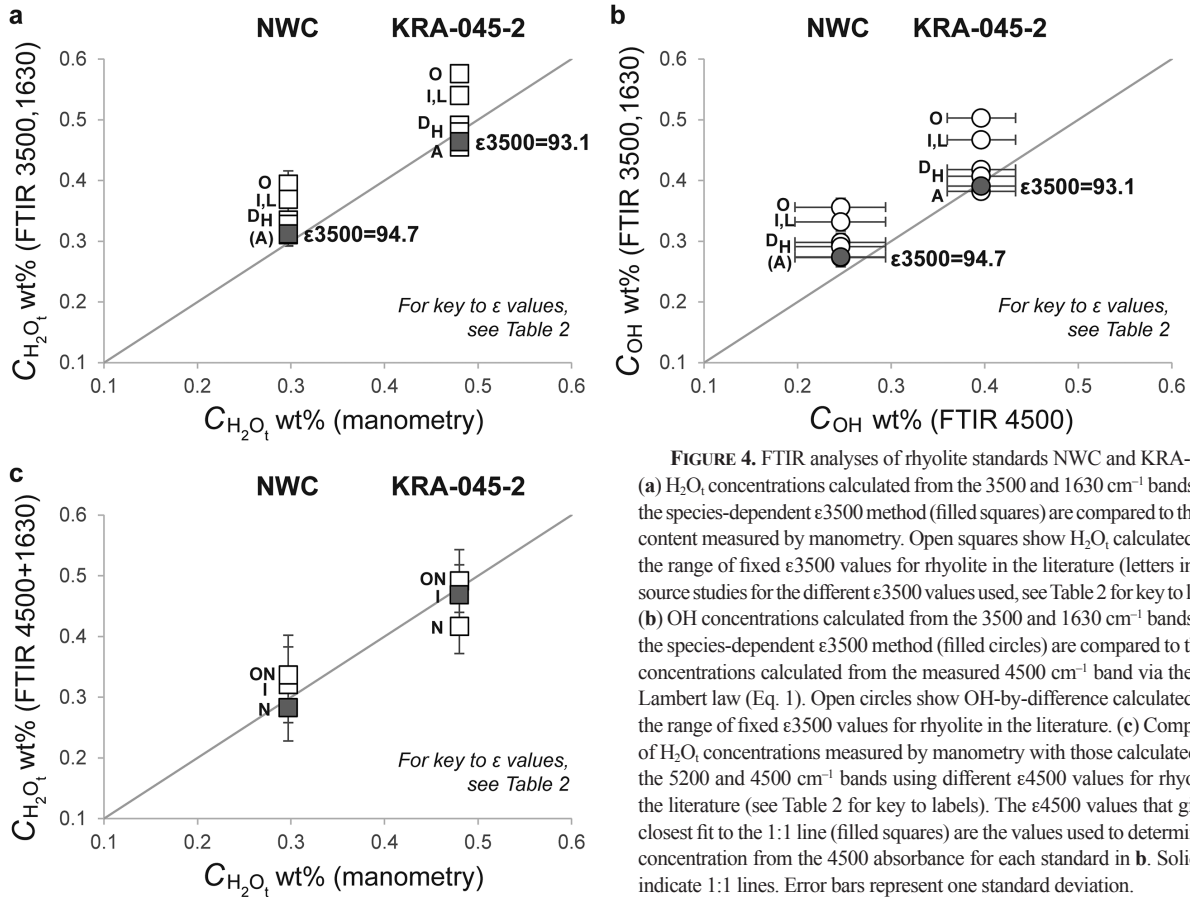


FIGURE 4. FTIR analyses of rhyolite standards NWC and KRA-045-2. (a) $\text{H}_2\text{O}_\text{T}$ concentrations calculated from the 3500 and 1630 cm^{-1} bands using the species-dependent ϵ_{3500} method (filled squares) are compared to the $\text{H}_2\text{O}_\text{T}$ content measured by manometry. Open squares show $\text{H}_2\text{O}_\text{T}$ calculated using the range of fixed ϵ_{3500} values for rhyolite in the literature (letters indicate source studies for the different ϵ_{3500} values used, see Table 2 for key to labels). (b) OH concentrations calculated from the 3500 and 1630 cm^{-1} bands using the species-dependent ϵ_{3500} method (filled circles) are compared to the OH concentrations calculated from the measured 4500 cm^{-1} band via the Beer-Lambert law (Eq. 1). Open circles show OH-by-difference calculated using the range of fixed ϵ_{3500} values for rhyolite in the literature. (c) Comparison of $\text{H}_2\text{O}_\text{T}$ concentrations measured by manometry with those calculated from the 5200 and 4500 cm^{-1} bands using different ϵ_{4500} values for rhyolite in the literature (see Table 2 for key to labels). The ϵ_{4500} values that give the closest fit to the 1:1 line (filled squares) are the values used to determine OH concentration from the 4500 absorbance for each standard in **b**. Solid lines indicate 1:1 lines. Error bars represent one standard deviation.

By contrast, the $\text{H}_2\text{O}_\text{T}$ concentration calculated for the rhyolite NWC (Fig. 4a) is only 0.015 wt% higher than the manometry value, but due to the low $\text{H}_2\text{O}_\text{T}$ content of this sample the relative difference is higher (5%). Possible sources of error include slight heterogeneity in water content between the chip that was analyzed with manometry and the chip that was analyzed with FTIR, and differences in how the baseline was picked for the 1630 cm^{-1} $\text{H}_2\text{O}_\text{m}$ peak (see below). Despite these minor discrepancies, the $\text{H}_2\text{O}_\text{T}$ and OH concentrations calculated using the species-dependent ϵ_{3500} method are markedly closer to the independently determined concentrations than some of the concentrations calculated using fixed ϵ_{3500} values from the literature, which may differ by up to 45% of the known values. Since using a fixed ϵ_{3500} value necessarily implies that OH concentration must be found as OH-by-difference, the resulting errors in $\text{H}_2\text{O}_\text{T}$ concentration are also propagated through as errors in OH concentration.

Accuracy of $\text{H}_2\text{O}_\text{m}$ measurement

Since the $\text{H}_2\text{O}_\text{m}$ concentration is needed to calculate the species-dependent ϵ_{3500} value, any error in the $\text{H}_2\text{O}_\text{m}$ concentration affects the calculated OH and $\text{H}_2\text{O}_\text{T}$ concentrations. When using the 3500 cm^{-1} band, the $\text{H}_2\text{O}_\text{m}$ concentration will generally be determined from the 1630 cm^{-1} band. The ϵ_{1630} value for rhyolite comes from Newman et al. (1986) (Table 2), who used the spectrum of an anhydrous equivalent of the glass to define the baseline when measuring 1630 cm^{-1} absorbances, in recognition

of the silicate peak at ~ 1600 cm^{-1} that can interfere with the 1630 cm^{-1} $\text{H}_2\text{O}_\text{m}$ peak and may cause the 1630 cm^{-1} absorbance to be overestimated if using a linear baseline. In lieu of an anhydrous piece of the same glass, we used a hand-drawn flexicurve baseline pinned to the baseline immediately adjacent to the 1630 cm^{-1} peak to account for non-linearity of the baseline. This flexicurve baseline gives an $\text{H}_2\text{O}_\text{m}$ concentration of 0.04 wt% (and subsequent $\text{H}_2\text{O}_\text{T}$ concentration of 0.31 wt%), compared to 0.06 wt% $\text{H}_2\text{O}_\text{m}$ (and 0.32 wt% $\text{H}_2\text{O}_\text{T}$) if a linear baseline is used. The good agreement of our flexicurve $\text{H}_2\text{O}_\text{m}$ concentration measurement with the $\text{H}_2\text{O}_\text{m}$ concentrations measured by Newman et al. (1986) for NWC (0.05 wt% using 1630 cm^{-1} band and 0.03 wt% using 5200 cm^{-1} band) validate our method of fitting the 1630 cm^{-1} baseline, and the small difference between our FTIR $\text{H}_2\text{O}_\text{T}$ concentration value and the manometry value (0.015 wt%) indicates that its impact is limited. The weak intensity of the ~ 1600 cm^{-1} silicate peak means that significant absorbance is restricted to thick sample wafers, while the relative importance of its interference with the 1630 peak is greatest for samples with low $\text{H}_2\text{O}_\text{m}$ concentrations (McIntosh et al. 2015). The error introduced by the 1630 cm^{-1} baseline will therefore be greatest for water-poor samples, but since these samples should contain predominantly OH the ultimate error on the calculated OH and $\text{H}_2\text{O}_\text{T}$ concentrations using the species-dependent ϵ_{3500} method will be limited.

The accuracy of the $\text{H}_2\text{O}_\text{m}$ measurement will also necessarily rely on the accuracy of the ϵ_{1630} value used to obtain it. When

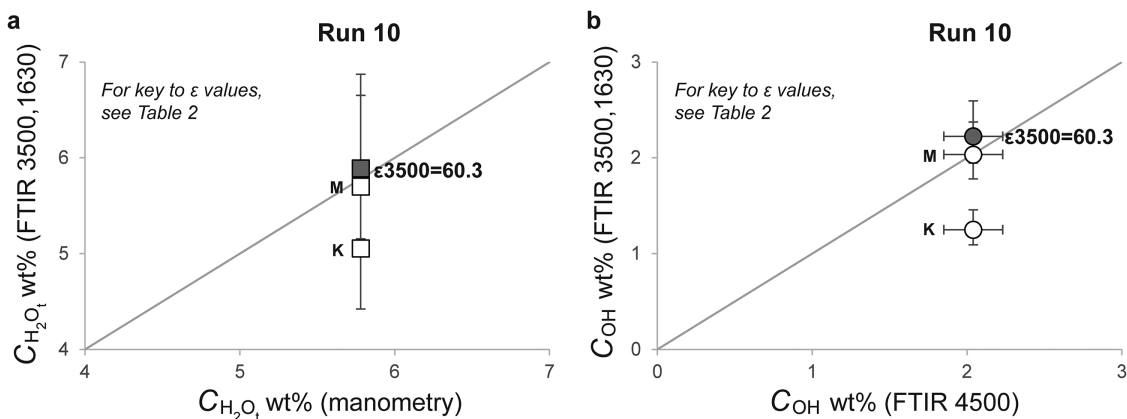


FIGURE 5. FTIR analysis of Fe-bearing andesite standard Run 10. **(a)** $\text{H}_2\text{O}_\text{T}$ concentration calculated from the 3500 and 1630 cm^{-1} bands using the species-dependent ϵ_{3500} method (filled square) is compared to the $\text{H}_2\text{O}_\text{T}$ content measured by manometry. Open squares show $\text{H}_2\text{O}_\text{T}$ calculated using the range of fixed ϵ_{3500} values for Fe-bearing andesite in the literature (letters indicate source studies for the different ϵ_{3500} values used, see Table 2 for key to labels). **(b)** OH concentration calculated from the 3500 and 1630 cm^{-1} absorbance bands using the species-dependent ϵ_{3500} method (filled circle) is compared to the OH concentrations calculated from the 4500 cm^{-1} band via the Beer-Lambert law (Eq. 1). Since the Run 10 sample was too thin to measure the 4500 cm^{-1} band we use instead the 4500 absorbance reported for this glass in Mandeville et al. (2002). Open circles show OH-by-difference calculated using the range of fixed ϵ_{3500} values for Fe-bearing andesite in the literature. Solid lines indicate 1:1 lines. Error bars are derived from the $\pm 3 \mu\text{m}$ error on the thickness measurement of this thin sample.

using the 3500 and 1630 cm^{-1} bands along with a fixed ϵ_{3500} value to find OH concentration as $\text{OH} = \text{H}_2\text{O}_\text{T} - \text{H}_2\text{O}_\text{m}$, the resulting error for the OH concentration may previously have been attributed to an inaccurate value of ϵ_{1630} , rather than ϵ_{3500} . We expect that the use of the species-dependent ϵ_{3500} method will reduce or remove such apparent discrepancies in H_2O species concentrations, and that the existing literature values for ϵ_{1630} in the compositions discussed in this paper will prove to be robust. It is worth noting that there is evidence that the ϵ values of the 5200 and 4500 cm^{-1} bands can vary with $\text{H}_2\text{O}_\text{T}$ concentration (Zhang et al. 1997b; Yamashita et al. 2008). The excellent fit of the $\text{H}_2\text{O}_\text{T}$ and OH concentrations calculated using the species-dependent ϵ_{3500} method to the published Newman rhyolite and Mandeville andesite data sets, which span a wide range of $\text{H}_2\text{O}_\text{T}$ concentrations, supports our assumption that the $\epsilon_{3500_{\text{H}_2\text{O}_\text{m}}}$ and $\epsilon_{3500_{\text{OH}}}$ values are true end-member values and do not themselves vary with $\text{H}_2\text{O}_\text{T}$ concentration. It is possible however that in the future a similar $\text{H}_2\text{O}_\text{T}$ -dependence will be found for ϵ_{1630} in some compositions, in which case we expect that our species-dependent ϵ_{3500} method can be adapted to account for it. As an example, we show that the $\text{H}_2\text{O}_\text{T}$ -dependent relationship derived for the 5200 cm^{-1} band by Zhang et al. (1997) can be successfully substituted into our method in place of the 1630 cm^{-1} band (see Supplementary¹ spreadsheet). In cases where both the 5200 and 1630 cm^{-1} bands can be measured for the same glass, we recommend using $\text{H}_2\text{O}_\text{m}$ concentrations calculated from both as input into Equation 4 to check and quantify possible error stemming from the $\text{H}_2\text{O}_\text{m}$ measurement.

Comparison of species-dependent ϵ_{3500} and fixed ϵ_{3500} values in literature

Since the true ϵ_{3500} value is species-dependent, the range in ϵ_{3500} values published in the literature results from the differences in the overall speciation (i.e., the ratio of OH to $\text{H}_2\text{O}_\text{m}$) of the samples used in the different calibration studies. In silicate melts and glasses, the two species interconvert according to the equilibrium reaction:



in which $\text{H}_2\text{O}_\text{m}$ reacts with bridging O atoms (O^{o}) to produce OH groups that are bound to the silicate framework (Stolper 1982a). For a given melt composition, the position of this equilibrium reaction (i.e., equilibrium speciation) is controlled by the temperature and $\text{H}_2\text{O}_\text{T}$ content (e.g., Stolper 1982a, 1989; Nowak and Behrens 1995; Behrens and Nowak 2003; Behrens and Yamashita 2008), with the equilibrium shifted toward OH at high temperature and low $\text{H}_2\text{O}_\text{T}$, and toward $\text{H}_2\text{O}_\text{m}$ at low temperature and high $\text{H}_2\text{O}_\text{T}$ (Fig. 6). Thus the true value of ϵ_{3500} will shift toward the higher $\epsilon_{3500_{\text{OH}}}$ end-member value for high temperatures and/or low $\text{H}_2\text{O}_\text{T}$ concentrations, and toward the lower $\epsilon_{3500_{\text{H}_2\text{O}_\text{m}}}$ end-member value for lower temperatures and/or high $\text{H}_2\text{O}_\text{T}$ concentrations. A final consideration is that the species interconversion reaction rate is strongly temperature dependent and slows dramatically during cooling (Zhang et al. 1991, 1995), until interconversion becomes negligible and speciation becomes “frozen in.” The temperature at which this occurs is termed the temperature of apparent equilibrium, T_{ae} , and for a given $\text{H}_2\text{O}_\text{T}$ content will be higher for a fast quench rate (since less time is available at every temperature interval for the reaction to approach equilibrium), and lower for a slow quench rate (e.g., Zhang et al. 1995; Xu and Zhang 2002). T_{ae} has been shown to be equivalent to the temperature of the glass

¹Deposit item AM-17-85952, Supplemental Material: A Microsoft Excel spreadsheet for using the species-dependent ϵ_{3500} method and for deriving new end-member ϵ_{3500} values from absorbance data. Deposit items are free to all readers and found on the MSA web site, via the specific issue’s Table of Contents (go to http://www.minsocam.org/MSA/AmMin/TOC/2017/Aug2017_data/Aug2017_data.html).

transition, T_g (Dingwell and Webb 1990; Zhang et al. 1997a). However, since T_g is most strictly defined as the glass transition temperature for a melt under a particular set of experimental conditions (e.g., a cooling rate of ~ 10 K/min), for clarity we use T_{ae} in the following discussion of samples with varied cooling histories. Thus the speciation of rapidly quenched samples will reflect their high T_{ae} by having higher $C_{\text{OH}}:C_{\text{H}_2\text{O}_\text{m}}$ ratios, hence higher ϵ_{3500} values, than equivalent samples with slower quench and lower T_{ae} .

The variation in published ϵ_{3500} values for a given glass composition therefore results from differences in both the water contents and temperature histories of the samples used in each calibration study. For Fe-bearing andesite, Mandeville et al. (2002) derived their fixed ϵ_{3500} value of 62.32 ± 0.42 from four glasses synthesized at 1030–1130 °C containing 0.21–4.32 wt% $\text{H}_2\text{O}_\text{i}$, with 39 of their 63 analyses stemming from their Run 9 glass (1030 °C, 4.32 wt% $\text{H}_2\text{O}_\text{i}$), while King et al. (2002) derived a fixed ϵ_{3500} value of 70.3 ± 6.86 using glasses synthesized at 1300 °C and containing 0–6.09 wt% $\text{H}_2\text{O}_\text{i}$, of which only three out of 43 analyses were made on glasses with >3.39 wt% $\text{H}_2\text{O}_\text{i}$. The higher ϵ_{3500} value of King et al. (2002) therefore likely reflects the lower average $\text{H}_2\text{O}_\text{i}$ content of their samples and their use of a higher experimental temperature and rapid quench rate (with samples quenched to below the glass transition in ~ 4 s), all of which favor higher $C_{\text{OH}}:C_{\text{H}_2\text{O}_\text{m}}$. Applying the fixed ϵ_{3500} value of King et al. (2002) to our measurements of the Fe-bearing andesite standard Run 10 underestimates the true $\text{H}_2\text{O}_\text{i}$ content of this glass by 0.72 wt% (Fig. 5a), highlighting the potential for large errors when applying a fixed ϵ_{3500} value to samples created under different conditions.

Our analyses of the rhyolite standards NWC and KRA-045-2 produced “true” ϵ_{3500} values of 94.7 and 93.1, respectively. These high ϵ_{3500} values reflect the dominance of OH at low $\text{H}_2\text{O}_\text{i}$ concentrations (Fig. 6), and are close to the highest fixed ϵ_{3500} values reported in the literature: 90 (Hauri et al. 2002) and 95 ± 8 (Aubaud et al. 2009). The calibration of Hauri et al. (2002) was based on a wide range of samples, the majority of which had <0.8 wt% $\text{H}_2\text{O}_\text{i}$, while that of Aubaud et al. (2009) was based on two samples with <0.16 wt% $\text{H}_2\text{O}_\text{i}$. At such low $\text{H}_2\text{O}_\text{i}$ contents only negligible $\text{H}_2\text{O}_\text{m}$ would be expected (Fig. 6) and it is therefore reasonable that these fixed ϵ_{3500} values should approach the end-member $\epsilon_{3500_{\text{OH}}}$ value of 100 ± 2 for rhyolite. Although Leschik et al. (2004) found that for glasses with >2 wt% $\text{H}_2\text{O}_\text{i}$ the ϵ_{3500} value decreases with increasing $\text{H}_2\text{O}_\text{i}$ concentration (as would be expected due to the increasing proportion of $\text{H}_2\text{O}_\text{m}$ and corresponding shift toward the lower $\epsilon_{3500_{\text{H}_2\text{O}_\text{m}}$ end-member), it is unclear why their fixed ϵ_{3500} value of 80 ± 4.9 for water-poor, OH-dominated samples (like our standards) is so much lower than both the Newman et al. $\epsilon_{3500_{\text{OH}}}$ end-member and other fixed ϵ_{3500} values.

By contrast the lowest published value for a fixed ϵ_{3500} value for rhyolite (75 ± 4) is that of Okumura et al. (2003), and is based on obsidian samples with 0.24–1.25 wt% $\text{H}_2\text{O}_\text{i}$ that were either unheated or heated to 500–700 °C. The authors noted that ϵ_{3500} values derived for the same obsidian source and $\text{H}_2\text{O}_\text{i}$ content (OBSW, 0.74 wt% $\text{H}_2\text{O}_\text{i}$) increased with the experimental temperature, being 73 for 500 °C, 76 for 600 °C, and 80 for 700 °C. As discussed by the authors, this variation can be explained by the temperature dependence of H_2O speciation that favors higher $C_{\text{OH}}:C_{\text{H}_2\text{O}_\text{m}}$, hence higher ϵ_{3500} , at higher temperatures. Okumura et al. (2003) also derived an ϵ_{3500} value for the original unheated

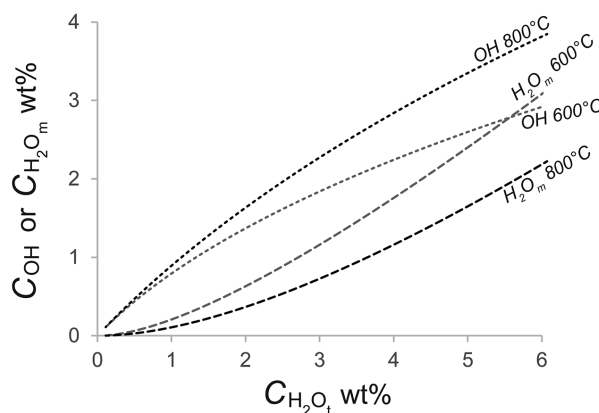


FIGURE 6. Example of experimentally determined water speciation model showing variation in OH and $\text{H}_2\text{O}_\text{m}$ concentration with $\text{H}_2\text{O}_\text{i}$ concentration at different temperatures for haplogranite composition (Nowak and Behrens 2001). OH is the dominant species at low- $\text{H}_2\text{O}_\text{i}$ concentrations and higher temperatures.

obsidian of 77 L/mol·cm. Based on their observed temperature dependence of ϵ_{3500} , we suggest that this value implies that the original T_{ae} of this obsidian was ~ 620 °C. While this indicates that finding the true ϵ_{3500} of a sample could be a useful method of finding its T_{ae} ($\approx T_g$), we stress that it is only valid if the temperature dependence of ϵ_{3500} is known for samples with exactly the same $\text{H}_2\text{O}_\text{i}$ content. Any derivation of a fixed value of ϵ_{3500} is effectively unique to samples with the exact same $\text{H}_2\text{O}_\text{i}$ content and temperature history, hence water speciation, as the samples that were used in its original calibration. Provided that end-member ϵ_{3500} values exist for the glass composition of interest, the advantage of our species-dependent ϵ_{3500} method is that it is possible to obtain accurate $\text{H}_2\text{O}_\text{i}$ and OH concentrations regardless of a sample’s $\text{H}_2\text{O}_\text{i}$ content or temperature history, and it can also account for changes in $\text{H}_2\text{O}_\text{i}$ concentration across an individual sample.

Application to hydrated samples

Volcanic glasses are susceptible to secondary hydration, i.e., the addition of water at low temperature in the time following eruption (Friedman and Smith 1958). Hydration of obsidian in particular has a long history of study, not only by the geological, but also the archaeological community, since diffusion modeling of hydration profiles at glass margins could offer a way to date obsidian flows or tools (e.g., Friedman and Long 1976, 1984; Anovitz et al. 1999; Riciputi et al. 2002). Recent studies have also demonstrated that secondary hydration is widespread and has altered the glass water contents of many erupted pyroclasts, with the effect most pronounced for samples with greater surface area exposed to outside water, such as vesicular glasses (e.g., Giachetti and Gonnermann 2013; Dingwell et al. 2015). Determining the original eruptive $\text{H}_2\text{O}_\text{i}$ content of hydrated glasses is therefore critical to volatile studies of erupted pyroclasts. Here we use an example of obsidian hydration from the literature to discuss how the species-dependent ϵ_{3500} method can be used to measure accurately the water species concentrations of hydrated glasses, with the potential to thereby reconstruct the original $\text{H}_2\text{O}_\text{i}$ contents of hydrated glasses.

Yokoyama et al. (2008) used transmission FTIR to analyze

hydration profiles at the margins of two obsidian flows from Kozushima, Japan, dated to 26 000 and 52 000 yr before present. Using the 3500 and 1630 cm^{-1} bands (and thus finding OH-by-difference), their analyses showed that both H_2O_m and H_2O_t concentrations increase toward the hydrated boundary. The trend in OH concentration was less simple, however, with OH either increasing or decreasing toward the boundary depending on the choice of the fixed ϵ_{3500} value. To prevent negative OH concentrations, they had to use a fixed ϵ_{3500} value of 60; much lower than any of the published values of ϵ_{3500} for rhyolite (Table 2). We extracted the concentration data from their published profiles and used their stated values of thickness and density to back-calculate their original 3500 and 1630 cm^{-1} absorbances using the Beer-Lambert law. We then applied our new species-dependent ϵ_{3500} method to their absorbances to recalculate the H_2O_t and OH concentrations of their hydration profiles, and to calculate the “true” ϵ_{3500} value for every point along the profile (Fig. 7). Doing so, we find that for both profiles the ϵ_{3500} value decreases toward the hydrated boundary. Accordingly, the OH concentration profiles no longer exhibit a fall to negative values and remain within 0.1 wt% of their non-hydrated values, while the increase in H_2O_t

concentrations toward the boundary becomes more pronounced than in the original profiles.

Since the species interconversion reaction effectively stops at the glass transition temperature (e.g., Dingwell and Webb 1990; Nowak and Behrens 1995; Zhang 1999; Behrens and Nowak 2003; Behrens and Yamashita 2008), water added at ambient temperature during secondary hydration is added as H_2O_m and not interconverted to OH; this creates “disequilibrium” speciation similar to that which develops during quench resorption (McIntosh et al. 2014). Glass in the hydrated margin becomes enriched in H_2O_m , and the correct ϵ_{3500} value to use will shift toward the $\epsilon_{3500_{\text{H}_2\text{O}_m}}$ end-member value (56 ± 2 for rhyolites). This explains why Yokoyama et al. (2008) had to use an ϵ_{3500} value of 60 to prevent negative OH concentrations when finding OH-by-difference. This value is much lower than the fixed ϵ_{3500} values in the literature, since the literature values were derived from samples with equilibrium rather than H_2O_m -rich disequilibrium speciation. When measuring H_2O_t and OH concentrations of hydrated samples using the 3500 cm^{-1} band, it is therefore imperative that the species-dependence of the ϵ_{3500} coefficient is accounted for.

The study of Yokoyama et al. (2008) was limited by the spatial

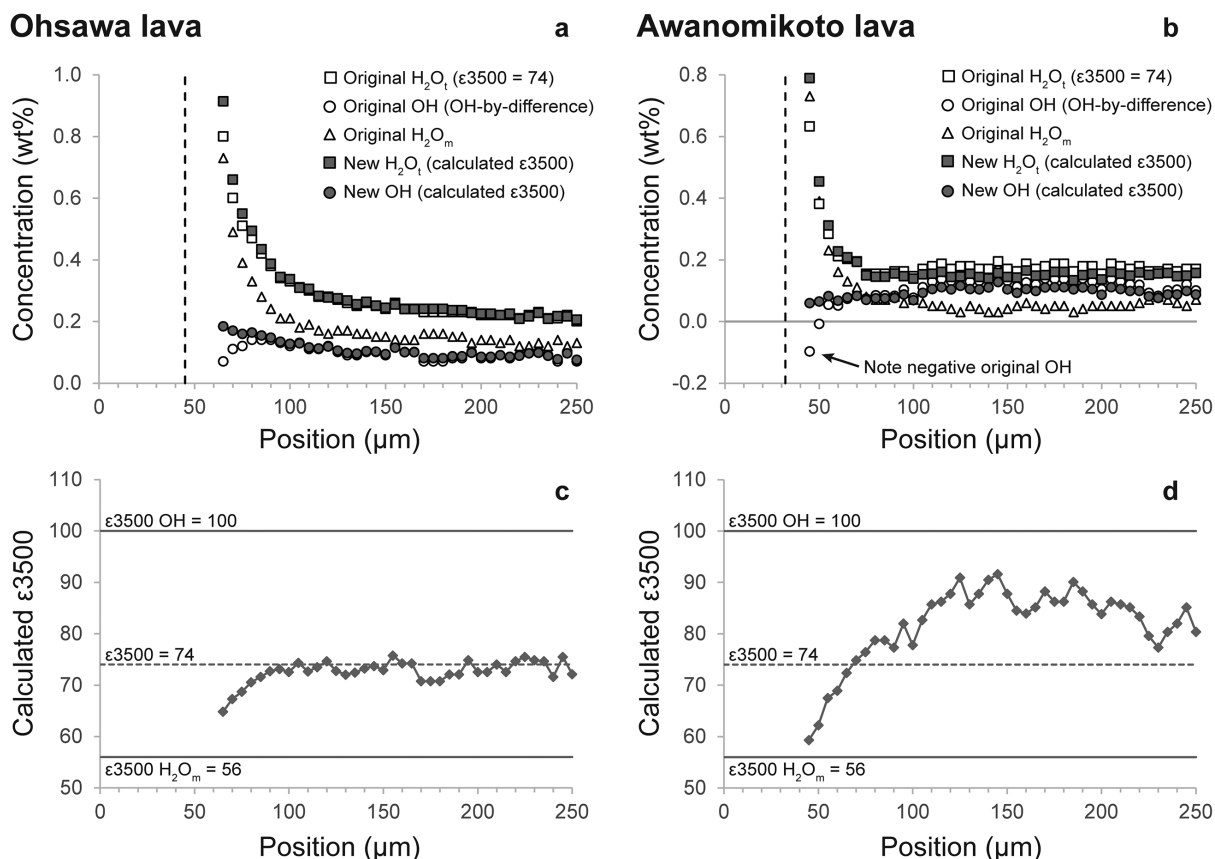


FIGURE 7. Recalculation of the obsidian hydration profiles published by Yokoyama et al. (2008) for (a) Ohsawa and (b) Awanomikoto lavas from Kozushima, Japan. The original profiles (open symbols) were obtained using a fixed value of $\epsilon_{3500} = 74$ and are shown alongside H_2O_t and OH profiles recalculated using the species-dependent ϵ_{3500} method (filled symbols). Note the negative OH values in the original Awanomikoto profile (b). The vertical black dashed lines represent the position of the glass edge; profiles are truncated where Yokoyama et al. (2008) calculated that there would be no contamination from the adjacent resin. (c and d) The “true” (species-dependent) ϵ_{3500} values calculated for each position in the recalculated profiles are shown with reference to the ϵ_{3500} end-member values for rhyolite and the original choice of fixed $\epsilon_{3500} = 74$.

resolution of their FTIR apparatus (they used $15 \times 50 \mu\text{m}$ spots at overlapping $5 \mu\text{m}$ steps) and we therefore truncate our recalculated profiles at the distance from the edge at which the authors calculated there would be no interference from the adjacent resin. FTIR apparatus with higher spatial resolution, such as those using a synchrotron source (e.g., von Aulock et al. 2014), may be able to investigate the concentration variations in hydrated margins in more detail. Nevertheless, it is clear from the data of Yokoyama et al. (2008) that OH concentration does not increase sharply in the hydration rim, whereas the H_2O_m concentration does, supporting their conclusion that the dominant species diffusing into the glass is H_2O_m . A recent study (Bindeman and Lowenstern 2016) on hydration of rhyolite during perlite formation at Yellowstone concluded that hydration occurred at temperatures $<200^\circ\text{C}$ but greater than ambient temperature, over an expected cooling timescale of weeks to years. The authors observed that, although dominated by addition of H_2O_m , this hydration also added minor amounts of OH ($-0.2 \text{ wt}\%$) to hydrated rims. Our recalculated hydration profile of Yokoyama et al.'s Ohsawa lava (Fig. 7a) reveals a slight increase in OH concentration from -0.1 to $-0.2 \text{ wt}\%$ toward the margin, raising the possibility that its hydration may have occurred under similar conditions to that of the Yellowstone perlite. However, for glasses that are quenched rapidly to ambient temperature and hydrated subsequently, it is expected that the OH content of a hydrated sample should remain the same as when that sample was first deposited. This is in keeping with observations of volcanoclastic glasses that contain hydrated regions. Those hydrated regions have elevated H_2O_m concentrations, but have similar OH concentrations to unhydrated regions of the same samples (e.g., Nichols et al. 2014). By using the new species-dependent ϵ_{3500} method to measure accurately the OH concentration of such hydrated glasses, it is now possible to estimate the original pre-hydration H_2O_i content by using speciation models (e.g., Nowak and Behrens 2001; Fig. 6) to find the H_2O_i concentration that corresponds to the measured OH concentration for the expected T_{ac} ($\approx T_g$) of the sample (e.g., Dingwell et al. 2015). Although the glass transition temperature can vary with cooling history and H_2O_i concentration, OH vs. H_2O_i curves for different values of T_g converge at low- H_2O_i concentrations (Fig. 6), making this an effective method for glasses with $<1 \text{ wt}\%$ OH. Other proposed methodologies for reconstructing the original H_2O_i content of hydrated glasses involve thermogravimetric analysis (TGA) (e.g., Denton et al. 2009, 2012; Tuffen et al. 2010; Giachetti et al. 2015) or hydrogen isotope analysis (e.g., DeGroot-Nelson et al. 2001)—both of which produce bulk measurements and destroy the sample—in conjunction with modeling of diffusion, for which some of the parameters are not well constrained for ambient temperatures. This FTIR methodology is relatively cheap and simple to perform, and has the significant benefit of permitting spatial variations in both the original and subsequent H_2O_i concentration to be measured.

Compositional dependence of the molar absorptivity coefficients

It has long been recognized that the values of FTIR molar absorptivity coefficients vary with glass composition (e.g., Silver et al. 1990; Dixon et al. 1995; Ohlhorst et al. 2001; Mandeville et al. 2002; Seaman et al. 2009; Mercier et al. 2010), hence it is unsurprising that the end-member ϵ_{3500} values also vary with

glass composition. H_2O_i and OH contents derived using the rhyolite end-member coefficients agree well with the manometry data for both of the rhyolite glass standards (Fig. 4), suggesting that these end-member ϵ_{3500} values are not sensitive to minor compositional differences, such as a few $\text{wt}\%$ of SiO_2 (Table 3), and can be successfully applied to other glasses with similar major element compositions. However, glasses with greater compositional differences will require their own set of end-member coefficients, as seen in the variation between values for rhyolite, albite, and Fe-bearing and Fe-free andesite (Table 2).

Previous studies have suggested that the molar absorptivity coefficients of the H_2O absorption bands decrease with decreasing tetrahedral cation fraction (τ) of the melt, where $\tau = (\text{Si}^{4+} + \text{Al}^{3+})/\text{total cations}$ (e.g., Dixon et al. 1995; Ohlhorst et al. 2001; Mandeville et al. 2002; Seaman et al. 2009; Mercier et al. 2010). Although our data are so far limited to only four glass compositions, our values of $\epsilon_{3500_{\text{OH}}}$ and $\epsilon_{3500_{\text{H}_2\text{O}_m}}$ do not show a trend with τ (Table 2), and neither do they show a trend with the ratio of non-bridging O atoms over tetrahedrally coordinated cations (NBO/T; Table 2). Although the end-member ϵ_{3500} values clearly vary with melt composition, it is not yet possible to simply link this variation with a particular structural parameter that describes the silicate melt.

Of the four compositions discussed here, the use of a species-dependent ϵ_{3500} is most important for the rhyolite and Fe-andesite compositions. These compositions have the greatest difference between the two end-member coefficients (56–100 and 49–79, respectively) hence the appropriate ϵ_{3500} value, and the calculated H_2O_i and OH concentrations, can vary widely. For Fe-free andesite the difference between the end-member coefficients is smaller (62–76) but is still sufficient to justify the use of species-dependent ϵ_{3500} . On the other hand, the difference between end-member ϵ_{3500} values for albite is so small (69–71) that they are within error of each other, which enabled Silver and Stolper (1989) to conclude that there is no advantage in choosing a species-dependent ϵ_{3500} value over a fixed ϵ_{3500} value for this composition.

IMPLICATIONS

Dissolved H_2O content exerts a strong control on silicate melt properties such as viscosity, glass transition temperature, diffusivities of mobile species, and crystallization kinetics. Consequently, for many studies throughout the geological, archeological, and materials sciences, it is critical to know accurately the H_2O contents of silicate glasses, even when the behavior of H_2O is not the main focus of the study. The relative ease of sample preparation and low cost of FTIR analyses means that, in many studies of this sort, the H_2O data are obtained by FTIR, and often by analyzing the 3500 cm^{-1} H_2O_i absorbance band. Our new species-dependent ϵ_{3500} method, which does not require a change in analytical procedure or expensive instrumentation, will improve the accuracy of these FTIR data, and remove systematic bias in samples that have undergone hydration. Previously published H_2O data that depend upon fixed ϵ_{3500} values will therefore need to be re-evaluated to identify and correct potential inaccuracies. This is particularly important given the common use of FTIR H_2O data to constrain glass standards used in the calibration of other analytical techniques such as SIMS (e.g., Hauri et al. 2002). We emphasize that this correction can be accomplished without the need for new instrumental analyses, by simply re-analyzing the raw absorbance,

thickness, and density data that have already been collected, using the methodology developed in this work. We provide a simple spreadsheet, which accepts these data and performs the relevant calculations, in the supplementary information¹.

The clear advantage of FTIR analysis over other techniques is the ability to obtain quantitative H_2O speciation data, which can be used to investigate topics such as the mechanisms and rates of H_2O diffusion (e.g., Zhang et al. 1991), or the pressure and temperature histories of glasses (e.g., Zhang et al. 1997a; McIntosh et al. 2014). Many of these studies involve measuring the spatial variation in H_2O species along an H_2O diffusion profile, for example along a diffusion couple experiment or toward a crack, bubble or crystal in the glass (e.g., Zhang et al. 1991; Castro et al. 2008; Berlo et al. 2013; von Aulock et al. 2013; McIntosh et al. 2014; Saubin et al. 2016; Watkins et al. 2017). In such cases, where H_2O_i concentration varies systematically with spatial position, it is essential to account for the species-dependence of ϵ_{3500} when using the 3500 cm^{-1} absorbance band, because otherwise errors will also vary systematically with spatial position, as illustrated by our reinterpretation of the Yokoyama et al. hydration profiles (Fig. 7). Removal of this systematic error will significantly improve the quality of interpretations of H_2O speciation data along such profiles.

As well as facilitating reanalysis and reinterpretation of existing studies of experimental and natural hydrous glasses, our new method also opens new avenues of research into glasses affected by secondary hydration. Secondary hydration has been shown to be a widespread phenomenon (e.g., Giachetti and Gonnermann 2013), and we recommend the use of FTIR analyses to identify (by their excess H_2O_m contents) glasses that have been hydrated; information that cannot be obtained by SIMS or Raman spectroscopy. Moreover, improved accuracy of H_2O speciation data along hydration profiles will benefit researchers investigating mechanisms of glass hydration, and the use of obsidian hydration profiles as a dating tool for volcanic and archaeological glasses. Most exciting of all, however, is the prospect of estimating the pre-hydration H_2O_i contents of hydrated glasses based on accurate measurement of their OH contents. We propose that this will be a particularly important breakthrough for understanding the eruption processes and associated hazards of silicic submarine eruptions, for which pyroclast glasses are routinely found to be hydrated (e.g., Bryant et al. 2003; Kutterolf et al. 2014). In the same way that the pressure-dependence of H_2O solubility can be used to determine paleo-ice thicknesses from subglacially erupted and quenched glasses (e.g., Tuffen et al. 2010), reconstructed H_2O_i contents of submarine pyroclast glasses can be used to establish the quench depth of unobserved submarine eruption plumes and, in particular, to determine whether pyroclasts now resting on the deep sea floor may have originally reached the sea surface (e.g., Fiske et al. 2001; Tani et al. 2008; Allen et al. 2010; Rotella et al. 2013).

Although this paper has focused necessarily on rhyolitic and andesitic glasses, it is hoped that future FTIR studies of hydrous silicate glasses will enable further sets of end-member ϵ_{3500} values to be derived for more compositions (particularly basalt). This will allow the species-dependent ϵ_{3500} method to be applied more widely, and will also improve our understanding of the composition dependence of molar absorptivity coefficients. Such future studies may also improve upon the molar absorptivity coefficients that are available to us today. This study has benefited

hugely from the previously published data sets of Newman et al. (1986) and Mandeville et al. (2002), which contained the absorbance, thickness, and density data necessary to test and develop our methodology. We therefore strongly advocate for researchers using FTIR data to publish, as we have done here, not only their concentration data but also the absorbance, thickness and density data that underpin them, with the aim of increasing the longevity and relevance of their hard-won data.

ACKNOWLEDGMENTS

We are grateful to Madeleine Humphreys for providing the glass standards used in this study. We thank Jake Lowenstern and an anonymous reviewer for their thorough and insightful reviews. This research was supported by a Japan Society for the Promotion of Science Postdoctoral Fellowship for Foreign Researchers held by I.M., and a JSPS Grant-in-Aid for Scientific Research (Kakenhi grant number 00470120) awarded to A.R.L.N and I.M.; E.W.L. acknowledges support from the U.K. Natural Environment Research Council via grant NE/N002954/1. Data Access Statement: Underlying data can be obtained by contacting the corresponding author.

REFERENCES CITED

- Allen, S.R., Fiske, R.S., and Tamura, Y. (2010) Effects of water depth on pumice formation in submarine domes at Sumisu, Izu-Bonin arc, western Pacific. *Geology*, 38, 391–394.
- Anovitz, L.M., Elam, J.M., Riciputi, L.R., and Cole, D.R. (1999) The failure of obsidian hydration dating: Sources, implications, and new directions. *Journal of Archaeological Science*, 26, 735–752.
- Anovitz, L.M., Cole, D.R., and Fayek, M. (2008) Mechanisms of rhyolitic glass hydration below the glass transition. *American Mineralogist*, 93, 1166–1178.
- Aubaud, C., Bureau, H., Raepsaet, C., Khodja, H., Withers, A.C., Hirschmann, M.M., and Bell, D.R. (2009) Calibration of the infrared molar absorption coefficients for H in olivine, clinopyroxene and rhyolitic glass by elastic recoil detection analysis. *Chemical Geology*, 260, 286–294.
- Baker, D.R., and Alletti, M. (2012) Fluid saturation and volatile partitioning between melts and hydrous fluids in crustal magmatic systems: The contribution of experimental measurements and solubility models. *Earth-Science Reviews*, 114, 298–324.
- Baker, D.R., Freda, C., Brooker, R.A., and Scarlato, P. (2005) Volatile diffusion in silicate melts and its effects on melt inclusions. *Annals of Geophysics*, 48, 699–717.
- Behrens, H., and Nowak, M. (2003) Quantification of H_2O speciation in silicate glasses and melts by IR spectroscopy—in situ versus quench techniques. *Phase Transitions*, 76, 45–61.
- Behrens, H., and Yamashita, S. (2008) Water speciation in hydrous sodium tetrasilicate and hexasilicate melts: Constraint from high temperature NIR spectroscopy. *Chemical Geology*, 256, 305–314.
- Berlo, K., Tuffen, H., Smith, V.C., Castro, J.M., Pyle, D.M., Mather, T.A., and Geraki, K. (2013) Element variations in rhyolitic magma resulting from gas transport. *Geochimica et Cosmochimica Acta*, 121, 436–451.
- Bindeman, I.N., and Lowenstern, J.B. (2016) Low- δD hydration rinds in Yellowstone perlitic record rapid syn-eruptive hydration during glacial and interglacial conditions. *Contributions to Mineralogy and Petrology*, 171, 89.
- Bryant, C.J., Arculus, R.J., and Eggins, S.M. (2003) The geochemical evolution of the Izu-Bonin arc system: A perspective from tephra recovered by deep-sea drilling. *Geochemistry, Geophysics, Geosystems*, 4, 1094.
- Castro, J.M., Beck, P., Tuffen, H., Nichols, A.R.L., Dingwell, D.B., and Martin, M.C. (2008) Timescales of spherulite crystallization in obsidian inferred from water concentration profiles. *American Mineralogist*, 93, 1816–1822.
- DeGroot-Nelson, P.J., Cameron, B.I., Fink, J.H., and Holloway, J.R. (2001) Hydrogen isotope analysis of rehydrated silicic lavas: implications for eruption mechanisms. *Earth and Planetary Science Letters*, 185, 331–341.
- Denton, J.S., Tuffen, H., Gilbert, J.S., and Odling, N. (2009) The hydration and alteration of perlitic and rhyolite. *Journal of the Geological Society*, 166, 895–904.
- Denton, J.S., Tuffen, H., and Gilbert, J.S. (2012) Variations in hydration within perlitised rhyolitic lavas—Evidence from Torfajökull, Iceland. *Journal of Volcanology and Geothermal Research*, 223–224, 64–73.
- Dingwell, D.B., and Webb, S.L. (1990) Relaxation in silicate melts. *European Journal of Mineralogy*, 2, 427–229.
- Dingwell, D.B., Lavallée, Y., Hess, K.-U., Flaws, A., Marti, J., Nichols, A.R.L., Gilg, H.A., and Schillinger, B. (2015) Eruptive shearing of tube pumice: Pure and simple. *Solid Earth Discussions*, 7, 3053–3085.
- Dixon, J.E., Stolper, E.M., and Holloway, J.R. (1995) An experimental study of water and carbon dioxide solubilities in mid-ocean ridge basaltic liquids. Part I: Calibration and solubility models. *Journal of Petrology*, 36, 1607–1631.
- Dobson, P., Epstein, S., and Stolper, E.M. (1989) Hydrogen isotope fractionation between coexisting vapor and silicate glasses and melts at low pressure. *Geochimica et Cosmochimica Acta*, 53, 2723–2730.
- Fiske, R.S., Naka, J., Iizasa, K., Yuasa, M., and Klaus, A. (2001) Submarine silicic caldera at the front of the Izu-Bonin arc, Japan: Voluminous seafloor eruptions

- of rhyolite pumice. *Bulletin of the Geological Society of America*, 113, 813–824.
- Friedman, I., and Long, W. (1976) Rate of obsidian hydration. *Science*, 191, 347–352.
- (1984) Volcanic glasses, their origins and alteration processes. *Journal of Non-Crystalline Solids*, 67, 127–133.
- Friedman, I., and Smith, R.L. (1958) The deuterium content of water in some volcanic glasses. *Geochimica et Cosmochimica Acta*, 15, 218–228.
- Giachetti, T., and Gonnermann, H.M. (2013) Water in volcanic pyroclast: Rehydration or incomplete degassing? *Earth and Planetary Science Letters*, 369–370, 317–332.
- Giachetti, T., Gonnermann, H.M., Gardner, J.E., Shea, T., and Gouldstone, A. (2015) Discriminating secondary from magmatic water in rhyolitic matrix-glass of volcanic pyroclasts using thermogravimetric analysis. *Geochimica et Cosmochimica Acta*, 148, 457–476.
- Giordano, D., Russell, J.K., and Dingwell, D.B. (2008) Viscosity of magmatic liquids: A model. *Earth and Planetary Science Letters*, 271, 123–134.
- Gualda, G.A.R., Ghiorso, M.S., Lemons, R.V., and Carley, T.L. (2012) Rhyolite-MELTS: a modified calibration of MELTS optimized for silica-rich, fluid-bearing magmatic systems. *Journal of Petrology*, 53, 875–890.
- Hammer, J.E. (2004) Crystal nucleation in hydrous rhyolite: Experimental data applied to classical theory. *American Mineralogist*, 89, 1673–1679.
- Hauri, E., Wang, J., Dixon, J.E., King, P.L., Mandeville, C., and Newman, S. (2002) SIMS analysis of volatiles in silicate glasses I. Calibration, matrix effects and comparisons with FTIR. *Chemical Geology*, 183, 99–114.
- Hess, K.-U., and Dingwell, D.B. (1996) Viscosities of hydrous leucogranitic melts: A non-Arrhenian model. *American Mineralogist*, 81, 1297–1300.
- Ihinger, P.D., Hervig, R.L., and McMillan, P.F. (1994) Analytical methods for volatiles in glasses. *Reviews in Mineralogy and Geochemistry*, 30, 67–121.
- King, P.L., Vennemann, T.W., Holloway, J.R., Hervig, R.L., Lowenstern, J.B., and Forneris, J.F. (2002) Analytical techniques for volatiles: A case study using intermediate (andesitic) glasses. *American Mineralogist*, 87, 1077–1089.
- Kutterolf, S., Schindlbeck, J.C., Scudder, R.P., Murray, R.W., Pickering, K.T., Freundt, A., Labanich, S., Heydolph, K., Saito, S., Naruse, H., and others. (2014) Large volume submarine ignimbrites in the Shikoku Basin: An example for explosive volcanism in the Western Pacific during the Late Miocene. *Geochemistry, Geophysics, Geosystems*, 15, 1837–1851.
- Le Losq, C., Cody, G.D., and Mysen, B.O. (2015) Complex IR spectra of OH⁻ groups in silicate glasses: Implications for the use of the 4500 cm⁻¹ IR peak as a marker of OH⁻ groups concentration. *American Mineralogist*, 100, 945–950.
- Leschik, M., Heide, G., Frischat, G.H., Behrens, H., Wiedenbeck, M., Wagner, N., Heide, K., Geissler, H., and Reinholz, U. (2004) Determination of H₂O and D₂O contents in rhyolitic glasses. *Physics and Chemistry of Glasses*, 45, 238–251.
- Malfait, W.J. (2009) The 4500 cm⁻¹ infrared absorption band in hydrous aluminosilicate glasses is a combination band of the fundamental (Si,Al)-OH and O-H vibrations. *American Mineralogist*, 94, 849–852.
- Mandeville, C.W., Sasaki, A., Saito, G., Faure, K., King, R., and Hauri, E. (1998) Open-system degassing of sulfur from Krakatau 1883 magma. *Earth and Planetary Science Letters*, 160, 709–722.
- Mandeville, C.W., Webster, J.D., Rutherford, M.J., Taylor, B.E., Timbal, A., and Faure, K. (2002) Determination of molar absorptivities for infrared absorption bands of H₂O in andesitic glasses. *American Mineralogist*, 87, 813–821.
- Maria, A.H., and Lühr, J.F. (2008) Lamprophyres, basanites, and basalts of the Western Mexican Volcanic Belt: Volatile contents and a Vein-Wallrock melting relationship. *Journal of Petrology*, 49, 2123–2156.
- McIntosh, I.M., Llewellyn, E.W., Humphreys, M.C.S., Nichols, A.R.L., Burgisser, A., and Schipper, C.I. (2014) Distribution of dissolved water in magmatic glass records growth and resorption of bubbles. *Earth and Planetary Science Letters*, 401, 1–11.
- McIntosh, I.M., Nichols, A.R.L., Schipper, C.I., and Stewart, B. (2015) Glass composition-dependent silicate absorption peaks in FTIR spectroscopy: Implications for measuring sample thickness and molecular H₂O. In *American Geophysical Union Fall Meeting* p. V23B–3092.
- Mercier, M., Di Muro, A., Métrich, N., Giordano, D., Belhadj, O., and Mandeville, C.W. (2010) Spectroscopic analysis (FTIR, Raman) of water in mafic and intermediate glasses and glass inclusions. *Geochimica et Cosmochimica Acta*, 74, 5641–5656.
- Newman, S., Stolper, E.M., and Epstein, S. (1986) Measurement of water in rhyolitic glasses: Calibration of an infrared spectroscopic technique. *American Mineralogist*, 71, 1527–1541.
- Nichols, A.R.L., Potuzak, M., and Dingwell, D.B. (2009) Cooling rates of basaltic hyaloclastites and pillow lava glasses from the HSDP2 drill core. *Geochimica et Cosmochimica Acta*, 73, 1052–1066.
- Nichols, A.R.L., Beier, C., Brandl, P.A., Buchs, D.M., and Krumm, S.H. (2014) Geochemistry of volcanic glasses from the Louisville Seamount Trail (IODP Expedition 330): Implications for eruption environments and mantle melting. *Geochemistry, Geophysics, Geosystems*, 15, 1–21.
- Nowak, M., and Behrens, H. (1995) The speciation of water in haplogranitic glasses and melts determined by in situ near-infrared spectroscopy. *Geochimica et Cosmochimica Acta*, 59, 3445–3450.
- (2001) Water in rhyolitic magmas: getting a grip on a slippery problem. *Earth and Planetary Science Letters*, 184, 515–522.
- Ohlhorst, S., Behrens, H., and Holtz, F. (2001) Compositional dependence of molar absorptivities of near-infrared OH⁻ and H₂O bands in rhyolitic to basaltic glasses. *Chemical Geology*, 174, 5–20.
- Okumura, S., and Nakashima, S. (2005) Molar absorptivities of OH and H₂O in rhyolitic glass at room temperature and at 400–600 °C. *American Mineralogist*, 90, 441–447.
- Okumura, S., Nakamura, M., and Nakashima, S. (2003) Determination of molar absorptivity of IR fundamental OH-stretching vibration in rhyolitic glasses. *American Mineralogist*, 88, 1657–1662.
- Riciputi, L.R., Elam, J.M., Anovitz, L.M., and Cole, D.R. (2002) Obsidian diffusion dating by secondary ion mass spectrometry: A test using results from Mound 65, Chalco, Mexico. *Journal of Archaeological Science*, 29, 1055–1075.
- Rotella, M.D., Wilson, C.J.N., Barker, S.J., and Wright, I.C. (2013) Highly vesicular pumice generated by buoyant detachment of magma in subaqueous volcanism. *Nature Geoscience*, 6, 129–132.
- Saubin, E., Tuffen, H., Gurioli, L., Owen, J., Castro, J.M., Berlo, K., McGowan, E.M., Schipper, C.I., and Wehbe, K. (2016) Conduit dynamics in transitional rhyolitic activity recorded by tuffsite vein textures from the 2008–2009 Chaitén Eruption. *Frontiers in Earth Science*, 4, 1–17.
- Seaman, S.J., Dyar, M.D., and Marinkovic, N. (2009) The effects of heterogeneity in magma water concentration on the development of flow banding and spherulites in rhyolitic lava. *Journal of Volcanology and Geothermal Research*, 183, 157–169.
- Silver, L.A., and Stolper, E. (1989) Water in albitic glasses. *Journal of Petrology*, 30, 667–709.
- Silver, L.A., Ihinger, P.D., and Stolper, E.M. (1990) The influence of bulk composition on the speciation of water in silicate glasses. *Contributions to Mineralogy and Petrology*, 104, 142–162.
- Stolper, E.M. (1982a) The speciation of water in silicate melts. *Geochimica et Cosmochimica Acta*, 46, 2609–2620.
- (1982b) Water in silicate glasses: An infrared spectroscopic study. *Contributions to Mineralogy and Petrology*, 81, 1–17.
- (1989) Temperature dependence of the speciation of water in rhyolitic melts and glasses. *American Mineralogist*, 74, 1247–1257.
- Tani, K., Fiske, R.S., Tamura, Y., Kido, Y., Naka, J., Shukumo, H., and Takeuchi, R. (2008) Sumisu volcano, Izu-Bonin arc, Japan: Site of a silicic caldera-forming eruption from a small open-ocean island. *Bulletin of Volcanology*, 70, 547–562.
- Tuffen, H., Owen, J., and Denton, J. (2010) Magma degassing during subglacial eruptions and its use to reconstruct palaeo-ice thicknesses. *Earth-Science Reviews*, 99, 1–18.
- Vetere, F., Behrens, H., Holtz, F., and Neuville, D. (2006) Viscosity of andesitic melts—New experimental data and a revised calculation model. *Chemical Geology*, 228, 233–245.
- von Aulock, F.W., Nichols, A.R.L., Kennedy, B.M., and Oze, C. (2013) Timescales of texture development in a cooling lava dome. *Geochimica et Cosmochimica Acta*, 114, 72–80.
- von Aulock, F.W., Kennedy, B.M., Schipper, C.I., Castro, J.M., Martin, D.E., Oze, C., Watkins, J.M., Wallace, P.J., Puskar, L., Bégué, F., and others. (2014) Advances in Fourier transform infrared spectroscopy of natural glasses: From sample preparation to data analysis. *Lithos*, 206–207, 52–64.
- Watkins, J.M., Gardner, J.E., and Befus, K.S. (2017) Nonequilibrium degassing, regassing, and vapor fluxing in magmatic feeder systems. *Geology*, 45, 183–186.
- Wohletz, K.H., and Heiken, G. (1992) *Volcanology and Geothermal Energy*. University of California Press.
- Wysoczanski, R., and Tani, K. (2006) Spectroscopic FTIR imaging of water species in silicic volcanic glasses and melt inclusions: An example from the Izu-Bonin arc. *Journal of Volcanology and Geothermal Research*, 156, 302–314.
- Xu, Z., and Zhang, Y. (2002) Quench rates in air, water, and liquid nitrogen, and inference of temperature in volcanic eruption columns. *Earth and Planetary Science Letters*, 200, 315–330.
- Yamashita, S., Behrens, H., Schmidt, B.C., and Dupree, R. (2008) Water speciation in sodium silicate glasses based on NIR and NMR spectroscopy. *Chemical Geology*, 256, 231–241.
- Yokoyama, T., Okumura, S., and Nakashima, S. (2008) Hydration of rhyolitic glass during weathering as characterized by IR microspectroscopy. *Geochimica et Cosmochimica Acta*, 72, 117–125.
- Zhang, Y. (1999) H₂O in rhyolitic glasses and melts: Measurement, speciation, solubility, and diffusion. *Reviews of Geophysics*, 37, 493–516.
- Zhang, Y., Stolper, E.M., and Wasserburg, G.J. (1991) Diffusion of water in rhyolitic glasses. *Geochimica et Cosmochimica Acta*, 55, 441–456.
- Zhang, Y., Stolper, E.M., and Ihinger, P.D. (1995) Kinetics of the reaction H₂O+O = 2OH in rhyolitic and albitic glasses: Preliminary results. *American Mineralogist*, 80, 593–612.
- Zhang, Y., Jenkins, J., and Xu, Z. (1997a) Kinetics of the reaction H₂O+O = 2OH in rhyolitic glasses upon cooling: Geospeedometry and comparison with glass transition. *Geochimica et Cosmochimica Acta*, 61, 2167–2173.
- Zhang, Y., Belcher, R., Ihinger, P.D., Wang, L., Xu, Z., and Newman, S. (1997b) New calibration of infrared measurement of dissolved water in rhyolitic glasses. *Geochimica et Cosmochimica Acta*, 61, 3089–3100.